JCTC Journal of Chemical Theory and Computation

Mechanism of the Ethylene Polymerization at Very High Pressure

Martina Mugnai,[†] Marco Pagliai,[†] Gianni Cardini,*[,†,‡] and Vincenzo Schettino[†,‡]

Laboratorio di Spettroscopia Molecolare, Dipartimento di Chimica, Universitá di Firenze, Via della Lastruccia 3, Sesto Fiorentino, and European Laboratory for Nonlinear Spectroscopy (LENS), Via Nello Carrara, Sesto Fiorentino, Italy

Received October 19, 2007

Abstract: The reaction of ethylene in condensed phases under high pressure has been investigated by ab initio molecular dynamics. Both disordered and crystalline samples have been simulated, and some insights on the reaction mechanism have been obtained. System size effects have been investigated for the disordered samples. A polymerization reaction occurs by an ionic mechanism. In both the disordered and the crystal phases, the reaction products obtained (linear chains in the disordered systems and branched chains in the crystal) are in qualitative agreement with the experiments.

1. Introduction

Unsaturated hydrocarbons have been known for a long time to spontaneously react when subjected to very high pressure and to transform into polymeric materials.[1–3] Recent experiments[4,5] have shown that, under appropriate control of the experimental conditions, the reaction can proceed along well-defined pathways, and high-quality (conformationally pure and crystalline) polymers can be obtained with potentially interesting physical and chemical properties. In the case of butadiene, the high-pressure polymerization of the liquid, under laser irradiation, has been reported to produce pure trans polybutadiene.[4,6] It has also been reported that the high-pressure polymerization of ethylene can result in a fully crystalline high-density polyethylene,[5] as revealed by spectroscopic and X-ray diffraction characterization. It has been shown that, when the compressed liquid monomer reactants are laser-irradiated at appropriate wavelengths, the pressure reaction threshold is quite significantly lowered, thus opening perspectives of practical technological applications of these novel synthetic procedures.

The mechanisms of high-pressure polymerization, and more in general high-pressure reactions, are not completely understood, even though some general concepts are well established.[1–3] In the first instance, high-pressure reactions will be governed by geometrical constraints. In fact, at very high pressures, significant potential barriers build up and hinder the molecular mobility and reorientations, and reactions involving minimum molecular displacements are favored (topochemical principle).[7] However, it is believed that the leading factor determining the reaction pathway is the substantial change of the electronic structure of the reactants occurring at high pressure.[8] This will include shifts and broadening of the electronic energy levels and, consequently, mixing of the ground and excited states and the population of higher electronic states that can be efficiently accomplished thermally. These effects can be conveniently investigated by first principles molecular dynamics that simultaneously considers the nuclear motion and the electron density fluctuations. Polymerization reactions have been deeply studied, mainly as catalytic processes,[9–11] and recently, also the problem of stereoselectivity has been modeled using ab initio molecular dynamics.[12]

Previous Car–Parrinello molecular dynamics simulations of reactions under high pressure[13–16] have enlighted a few problems. First of all, the computed pressure is higher than the experimental counterpart due to the lack of long-range dispersive contributions (negative), since this kind of interaction is strongly underestimated by currently available exchange-correlation functionals in the generalized gradient approximation framework.[17] Furthermore, to observe a reaction induced by pressure in the typical time scale of an

* Corresponding author e-mail: gianni.cardini@unifi.it.
[†] Universitá di Firenze.
[‡] European Laboratory for Nonlinear Spectroscopy.

10.1021/ct700275v CCC: $40.75
Published on Web 02/27/2008

ab initio simulation, the system is overpressurized to speed up the process.

In the present work, we report on Car–Parrinello[18] molecular dynamics simulation of the polymerization at a high pressure of ethylene both in the liquid and in the solid phase. This is an interesting study case for high-pressure polymerization. In fact, while from the liquid,[5] as mentioned above, a linear polymer with no branching is obtained, the reaction of the solid[19] produces a substantially branched polymer at higher pressures, thus exposing the effects of geometrical constraints on the reaction mechanism. It will be shown that, even if the size of the simulated sample is small, the essentials of the high-pressure polymerization mechanisms can be extracted from the simulation in good agreement with experiments. In particular, it will be shown that, in the crystal, the anisotropy of the compressibility is responsible for the change from a linear to a nonlinear growth of the polymer.

2. Computational Details

Ab initio molecular dynamics calculations have been performed on ethylene samples in the liquid and crystal phases. Calculations in the liquid were carried out in cubic boxes of different sizes with 27 and 52 molecules to check for the effects of the sample size. The two initial samples were obtained by fully randomized samples obtained with classical molecular dynamics for rigid molecules[20] interacting with a Buckingham potential.[21] The ab initio simulations were started with a box of 13 Å for the sample with 27 molecules. Due to the higher memory requirements, the ab initio simulation for the larger sample was started with an initial box of 12 Å. In the case of the crystal, the initial simulation box is made up of a $3 \times 2 \times 3$ unitary monoclinic ($P = 20$ bar; $T = 90$ K; $P2_1/n$; lattice constants: $a = 4.613$, $b = 6.610$, $c = 4.037$ Å, $\beta = 94.54$ °, $Z = 2$)[22] cell with 36 molecules.

All of the calculations have been carried out by using BLYP[23,24] functional in the framework of the Car–Parrinello molecular dynamic method (CPMD).[18,25] Periodic boundary conditions (PBC) have been used. In order to check whether the reaction mechanism is ionic or radicalic, the simulations have been carried out with both the restricted and spin density formalisms. In the latter case, the simulations have also been repeated starting from a configuration close to the onset of the reaction, performing a random initialization of the wave function to prevent the electron coupling which could affect the observed reaction mechanism. As in previous studies,[15,26] a 40 Ry cutoff has been used for the plane-wave expansion limited to the Γ point. In the case of the spin density calculations in the crystal, the cutoff has been extended up to 60 Ry. Norm conserving Martins−Troullier[27] (radius = 1.0 au) and Car−von Barth[28] pseudo-potentials have been adopted for carbon and hydrogen atoms, respectively.

The evaluation of the pressure (calculated by using the stress tensor) can be affected by a large uncertainty due to Pulay forces effects, which are present in a variable-cell simulation. Therefore, we found it more convenient to refer to the volume or density of the simulated sample.

A thermal bath has been applied to the system by using the Nosé−Hoover chain method.[29–31] As usual, the bath parameters have been chosen by a trial-and-error procedure, after inspection of the power spectra of the atomic velocities autocorrelation function, in order to ensure a good coupling to the vibrational motions and a decoupling between electronic and nuclear degrees of freedom.

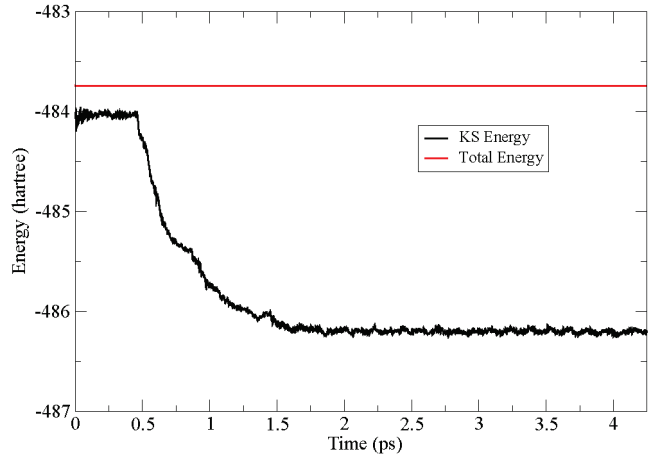

Figure 1. Evolution of the Kohn–Sham energy in the crystal sample during the reaction.

In the case of the reaction in the crystal, the bath has also been applied to the electrons (a bath frequency of 1500 and 4500 cm^{-1} has been chosen for the ions and the electrons, respectively; a kinetic energy of 0.04 au, corresponding to the average value of a simulation for unreacting crystals, has been chosen for the electrons). The goodness of this choice can be appreciated from Figure 1, showing that the Hamiltonian does not change appreciably along the simulation run even if the Kohn–Sham (KS) energy show a large variation.

To facilitate the analysis of the reaction mechanism, the simulations were performed in the NVT ensemble ($T = 300$ K, bath frequency 400 cm^{-1}, three thermostats). To compress the system, simulations in the NPT ensemble were performed (isotropic cell simulations with a cell mass of 1200 au) with an increasing external pressure between subsequent NVT simulations.

The various steps of the reaction pathway have been characterized calculating the maximally localized Wannier functions,[32–34] which are obtained by minimizing the spread of the Wannier functions (w_n) in direct space:

$$S = \sum_{n=1}^{N} \left(\langle w_n | r^2 | w_n \rangle - \langle w_n | \mathbf{r} | w_n \rangle^2 \right) \quad (1)$$

The implementation of this formula in the CPMD code is in the reciprocal space:[35]

$$S = \frac{2}{(2\pi)^2} \sum_{n}^{N_{\text{states}}} \sum_{I} \omega_I (1 - |z_{I,n}|) + O\left[\left(2\pi \hat{g}_1^{\text{t}} \times \overleftrightarrow{\mathbf{H}}^{-1} \right)^2 \right] \quad (2)$$

$$z_{I,n} = \int_V \mathrm{d}r \exp[i\mathbf{G}_I \times \mathbf{r}] |w_n(\mathbf{r})|^2 \quad (3)$$

where $\mathbf{H}$ is the transformation matrix from the crystallographic to the orthogonalized reference system and t, as

usual, indicates the transpose. The reciprocal vectors are $\mathbf{G}_I = 2\pi\ (\overleftrightarrow{\mathbf{H}}^{-1})^{\ t} \times \hat{g}_I$, where $\hat{g}_I$ represents the smallest independent Miller indeces, and they are determined along with their weights, ω_I,[35] by

$$\sum_{\mu=1}^{3} \overleftrightarrow{\mathbf{H}}^{t}_{\alpha\mu} \overleftrightarrow{\mathbf{H}}_{\mu\beta} = g_{\alpha\beta} = \sum_{I} \omega_I \hat{g}_{\alpha I} \hat{g}_{\beta I} \tag{4}$$

In eq 4, ω_I represents weights defined on the basis of the crystal symmetry, and the index I runs to a maximum value of 6 for triclinic crystals.

An analysis of the maximally localized Wannier functions has been performed adopting both a spin density and a restricted approach to verify that α and β spins were characterized by the same center and to rule out the radicalic mechanism.

3. Results and Discussion

3.1. Reactivity in the Liquid Phase. A major problem in ab initio studies of polymerization reactions under high pressure can be the dependence of the computed properties on the small system size necessarily adopted in the simulations. In particular, it is important to determine if and how geometrical properties, dipole moments, reaction mechanisms, and final products are affected by this parameter. To this aim, two ethylene samples made up of 27 (sample A) and 52 (sample B) molecules have been studied at the same density. Initially, the conditions for reactivity of the smaller sample A were found. The simulation box was compressed to 8.99 Å a side, which corresponds to a density of about 1.97 g cm^{-1}.

The reaction can be followed through the changes of the KS behavior reported in Figure 2, sample A.

Initially, the KS energy is almost constant, indicating that the system does not react. After 0.75 ps, an energy drop is observed, but the reaction immediately stops and only after a further 0.80 ps starts again, giving a polymeric chain. When the KS energy of the B sample (Figure 2) is observed, the absence of the initial plateau and an immediate energy drop can be noted. This can be explained considering that the polymerization reaction under high pressure is induced by thermal fluctuations which become more probable upon increasing the sample size. This leads to the hypothesis that, when the sample size is increased, the reaction can occur at lower densities. A simulation with the 52-molecule sample has also been carried out at a density of 1.91 g cm^{-3} (box side 11.27 Å; sample C). Also, in this sample, a reaction is observed but the associated energy decrease is smaller than for the other samples. In fact, in this case, the reaction immediately stops. The explanation of this behavior will be discussed in the following.

The compression procedure has been performed in steps. After each compression step, the system has been studied at constant volume. The data reported in the present work represent a selection made of significant phase space points to show the trend with increasing density. For sample A, three points have been selected for densities where reactions have not been observed (0.68, 1.47, and 1.72 g cm^{-3}). The fourth point (density of 1.97 g cm^{-3}) corresponds to the

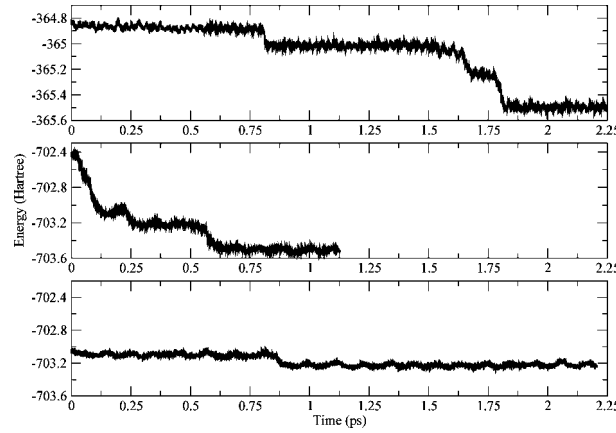

Figure 2. Kohn–Sham energy for three different samples. Parts A, B, and C (see text) go from top to bottom. Samples A and B show more evident drops in energy, corresponding to different reaction events occurring in the sample.

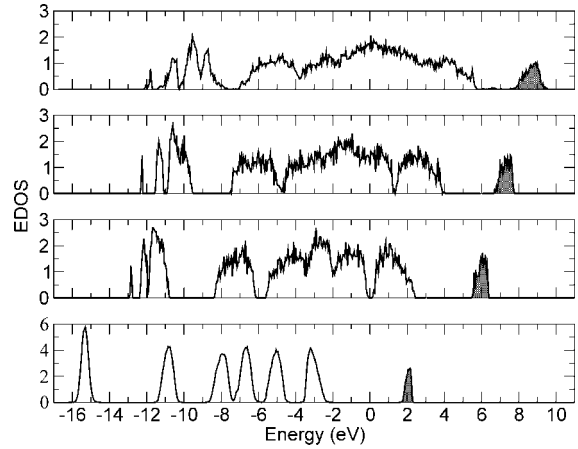

Figure 3. Kohn–Sham eigenvalues for decreasing cell size. The size of the cubic box for samples with 27 molecules from the bottom to the top are 12.8, 9.93, 9.42, and 8.99 Å.

density where the reaction has been observed. For these densities, the electronic density of states (EDOS) has been calculated, and the results for sample A are shown in Figure 3. For the higher-density sample, the calculation of the EDOS was reported before the occurrence of the first reactive event.

The EDOS has not been found to depend significantly on the sample size, except for a normalization factor. It can be seen from the figure that the EDOS continuously broadens with increasing density, thus making the mixing of states possible even by thermal fluctuations. At the highest density, the appearance of states in the HOMO–LUMO gap can be noted. It is to be stressed that these occupied and unoccupied states appear before the occurrence of the first reactive event and are essentially related to the strong molecular distortions that occur in a prereactive system.

The changes in the electron distribution induced by the pressure can be monitored by the electric dipole moment. Since for the reaction mechanism the dipole moment before the onset of the reaction is of interest, calculations were carried only for samples A and C, where the reaction occurs after a sufficiently long simulation time. The distribution of the dipole moment is shown in Figure 4.

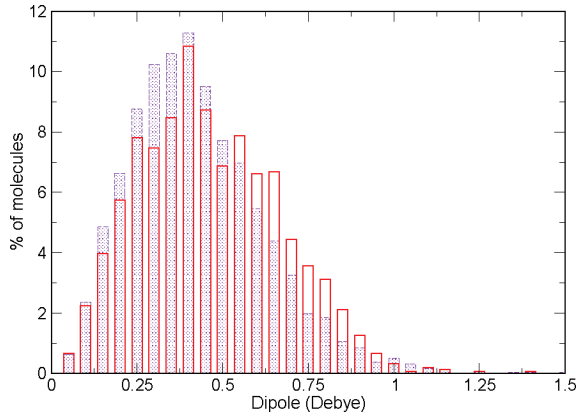

Figure 4. Molecular dipole distribution calculated before reaction in the A (red) and C (blue) samples.

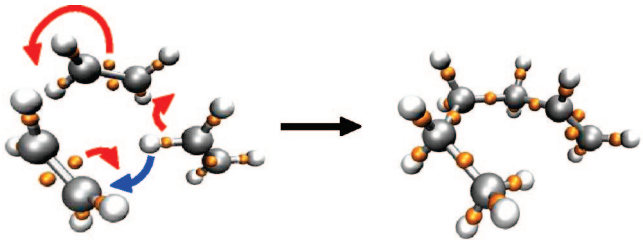

Figure 5. Reaction mechanism for the formation of a trimer. The small spheres depict the position of the WFCs.

The small difference between the two samples should not be ascribed to their size but rather to the different densities. The charge separation effect and transformation of an initially apolar into a polar molecule is a typical response of a system to pressure since this ensures a closer packing of the units (electrostriction). The present results confirms previous observations in high-pressure simulations of propylene[26] and butadiene.[15] The sample polarization suggests that the high-pressure polymerization mechanism is ionic. This conclusion is reinforced by the calculation of the centers of the maximally localized Wannier functions as shown in Figure 5.

The generation of a molecular dipole moment implies a transient geometrical deformation anticipating the change from sp^2 to sp^3 hybridization of the C atoms. This intermediate transformation preceding the reaction is independent from sample size. As shown by Boero et al.[12] in their study of propene polymerization, the use of Wannier function centers (WFC) is very useful to depict the reaction mechanism with the breaking and forming of chemical bonds.

As to the reaction products obtained in the simulation, we focus the discussion on the samples at higher density (A and B). Only a linear head-to-tail condensation of the monomeric units is observed. This is a relevant result since it is in agreement with experimental findings,[5] showing that the high-pressure polymerization of liquid ethylene produces a linear polymer and, under laser irradiation, even a completely crystalline material. The termination of the chain growth invariably occurs with the formation of $-CH{=}CH_2$ and $CH_3{-}CH_2-$ end groups, which implies an intramolecular hydrogen transfer in the forming oligomer. At the end of the simulation, 44% and 38% of the molecules have reacted in samples A and B, respectively. As a matter of fact, in several experiments, it has been found that at any given pressure the reaction may proceed only incompletely.[2] The incomplete sample transformation should most likely be ascribed to the drop, as the reaction proceeds, in pressure below a reaction threshold. This has been confirmed by a constant pressure simulation on one of the samples with 27 molecules where the reaction further proceeded with the formation of longer chains, and when the simulation was completed, the final products contained a chain with 18 and a chain with 16 carbon atoms, with two smaller oligomers (with four and six C atoms) and only five unreacted molecules. No attempts have been made to check the stability of these chains upon relaxation of the pressure since the molecules obtained appear to be stable species and, furthermore, the molecules extend through the PBC, and this can give rise to spurious effects when a decompression is performed.

Considering the reaction products in more detail, in sample A, two pentamers and one dimer are obtained, while in sample B a decamer, a pentamer, a trimer, and a dimer are produced. In the case of sample C, only the formation of a linear trimer (1-hexene) is observed. This simply implies that in this case the sample density is very close to the reaction threshold.

3.2. Reactivity in the Crystal. The molecular dynamics simulation shows that upon applying pressure the compressibility of the ethylene crystal is highly anisotropic. At the end of the NPT simulation, a final volume of 800 $Å^3$ (the simulation cell parameters are 9.825, 8.7, and 9.375 Å and $\beta = 93.4°$) was reached with a contraction of the b axis by 34.2% in comparison with a contraction by 29.3% and 22.5% for the a and c axes, respectively. The high-pressure structure is however still monoclinic with only a small variation of the β angle. The shortest intermolecular C−C distance between equivalent molecules is initially along the a axis and, from the initial value of 3.66 Å, reduces to 2.36 Å, whereas the shortest C−C distance between nonequivalent molecules reduces to 2.567 Å from 3.88 Å. These short intermolecular distances will allow a very fast reaction induced by thermal motion.

The high-pressure structure was the starting configuration for a subsequent NVT simulation. After 0.5 ps, a large single-step variation of the Kohn–Sham energy is observed and a reaction occurs involving two steps. First, a dimer is formed, and later, there is a growth of the chain. Initially, the reaction involves molecules on equivalent sites along the a crystallographic axis, leading to the formation of linear chains. In a later stage, nonequivalent molecules in the unit cell also participate in the reaction, with the formation of a branched polymeric chain. This result is in very nice agreement with experiments at high pressures (3.5 GPa)[19] showing, by a kinetic analysis according to Avrami's law,[36,37] that the polymer growth is linear in the initial stages and becomes nonlinear at later stages. In Figure 6, a snapshot of the simulation is reported, showing the formation of a linear and a branched polymeric chain. The two chains are longer than the simulation box parameters and therefore propagate through the periodic boundary conditions; this can be a

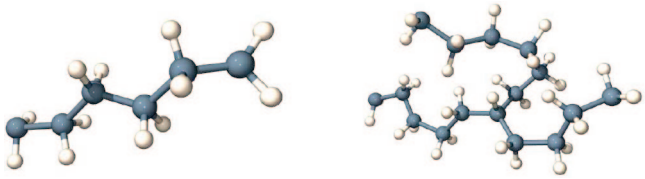

Figure 6. Linear and branched chains obtained in the high-pressure reaction simulations in crystalline ethylene.

source of spurious effects if the stability of the chains is studied upon relaxation of the pressure.

An indication of the electronic reorganization and of the reaction mechanism is obtained from the Wannier functions. In Figure 7a, a molecular orbital localized on the ethylene molecules on equivalent sites is represented. The orbital shows the presence of electron density between neighboring carbons laying along the same axis. This behavior represents an explanation for the formation of the linear chains. In fact, from a configuration of the crystal before the reaction occurs (see Figure 7b), it is possible to note once again the presence of this orbital (even if at higher energy). However, the electron density is localized also between two carbon atoms of ethylene molecules in nonequivalent sites. This allows for the propagation of the reaction along two different selected directions and determines the formation of branched chains. The above outlined mechanism can be considered typical of a crystal and can be attributed to collective motions of the molecules; this make this reaction mechanism quite different from the one described in the disordered system.

4. Conclusion

The reaction of ethylene induced by pressure has been found to proceed by an ionic mechanism and to be induced by thermal fluctuations. This suggests that the reaction can be obtained after the same short time at lower densities using larger samples with respect to those employed in this work. As expected, the KS density of states has been found to be strongly modified at high densities. The reactive system is characterized by a strong reduction of the HOMO–LUMO gap and a collapse of the higher occupied states in only one band. The molecules under high pressure are strongly deformed and show appreciable dipole moments supporting the electrostriction interpretation of the sample response to pressurization and an ionic reaction mechanism.

In the liquid, the formation of only linear polymeric chains is observed, in nice agreement with experiments. The length of the chain is limited by the reduction of pressure due to the condensation of the monomeric units and by the sample size. In the crystal, the anisotropy of the compressibility is evidenced, and the shortest C−C intermolecular contacts along the *a* axis and along the unit cell diagonal become comparable. As a consequence, the reaction in the solid proceeds in two steps. Initially, the polymerization along the *a* axis produces linear chains, but in a second stage, the onset of condensation along the diagonal leads to branched chains. The close agreement with experiments shows that the use of ab initio simulations in the Car–Parrinello approach is a quite reliable method to study the mechanism of this kind of reaction at high pressures.

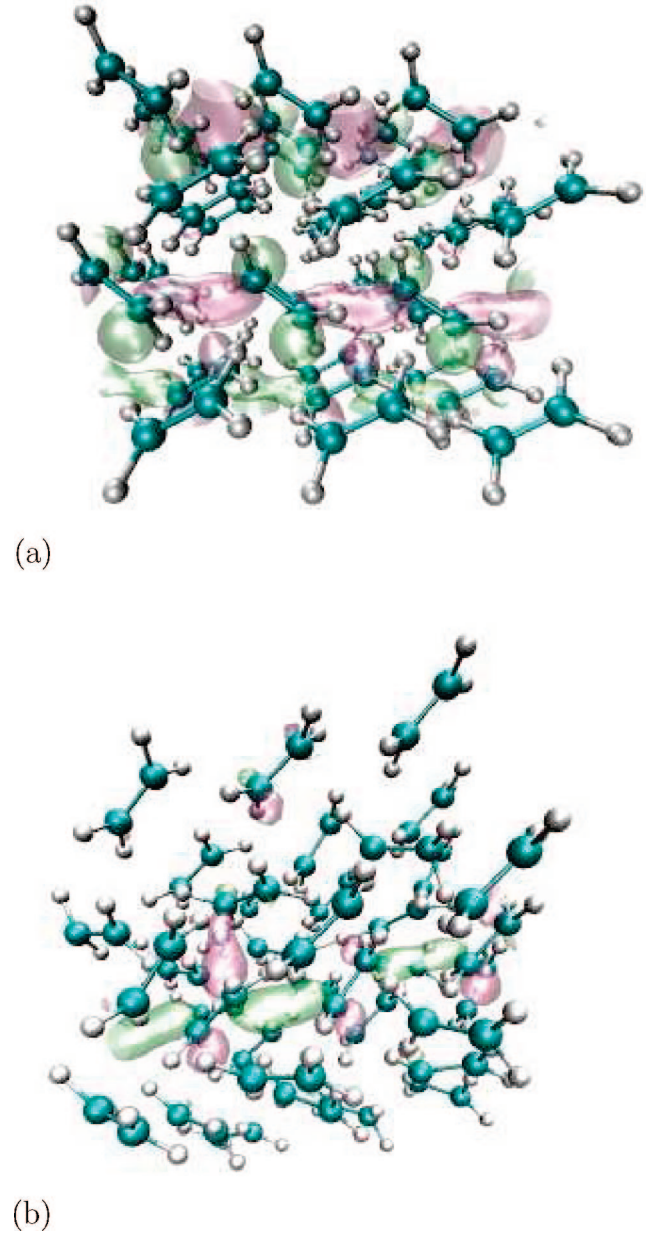

Figure 7. Bonded localized Wannier orbital (a) in the crystal at high pressure and (b) before the reaction starts.

In both systems studied by the analysis of the Wannier centers and the KS eigenvalues, it has been possible to rule out the radicalic mechanism under the thermodynamic conditions examined. The ionic mechanism has been found as in previous simulations on similar systems.[14,15] In the crystal, the polymerization occurs with a collective motion of the molecules.

Acknowledgment. The authors would like to thank Prof. Michele Parrinello, for helpful discussions. This work was supported by the Italian Ministero dell'Istruzione, dell'Universita e della Ricerca Scientifica e Tecnologica (MIUR).

References

(1) Schettino, V.; Bini, R. *Phys. Chem. Chem. Phys.* **2003**, *5*, 1951–1965.

(2) Schettino, V.; Bini, R.; Ceppatelli, M.; Ciabini, L.; Citroni, M. *Adv. Chem. Phys.* **2005**, *131*, 105–242.

(3) Schettino, V.; Bini, R. *Chem. Soc. Rev.* **2007**, *36*, 869–880.

(4) Citroni, M.; Ceppatelli, M.; Bini, R.; Schettino, V. *Science* **2002**, *295*, 2058–2060.

(5) Chelazzi, D.; Ceppatelli, M.; Santoro, M.; Bini, R.; Schettino, V. *Nat. Mater.* **2004**, *3*, 470.

(6) Bini, R. *Acc. Chem. Res.* **2004**, *37*, 95–101.

(7) Cohen, M. *Angew. Chem., Int. Ed.* **1975**, *14*, 386.

(8) Drickramer, H.; Frank, C. *Electrostatic transitions and the high pressure chemistry and physics of solids*; Chapman and Hall: London, 1973.

(9) Boero, M.; Parrinello, M.; Terakura, K. *J. Am. Chem. Soc.* **1998**, *120*, 2746–2752, and references therein.

(10) Vanka, K.; Xu, Z.; Seth, M.; Ziegler, T. *Top. Catal.* **2005**, *34*, 143–164.

(11) Kim, S.; Somorjai, G. *Proc. Natl. Acad. Sci. U.S.A.* **2006**, *103*, 15289–15294.

(12) Boero, M.; Parrinello, M.; Hüffer, S.; Weiss, H. *J. Am. Chem. Soc.* **2000**, *122*, 501–509, and references therein.

(13) Bernasconi, M.; Chiarotti, G. L.; Focher, P.; Parrinello, M.; Tosatti, E. *Phys. Rev. Lett.* **1997**, *78*, 2008–2011.

(14) Mugnai, M.; Cardini, G.; Schettino, V. *J. Chem. Phys.* **2004**, *120*, 5327–5333.

(15) Mugnai, M.; Cardini, G.; Schettino, V. *Phys. Rev. B: Condens. Matter Mater. Phys.* **2004**, *70*, 020101(1–4).

(16) Ciabini, L.; Gorelli, F. A.; Santoro, M.; Bini, R.; Schettino, V.; Raugei, S. *Nat. Mater.* **2007**, *6*, 39–43.

(17) Raugei, S.; Cardini, G.; Schettino, V. *Mol. Phys.* **1998**, *95*, 477–482.

(18) Car, R.; Parrinello, M. *Phys. Rev. Lett.* **1985**, *55*, 2471–2474.

(19) Chelazzi, D.; Ceppatelli, M.; Santoro, M.; Bini, R.; Schettino, V. *J. Phys. Chem. B* **2005**, *109*, 21658.

(20) Ciccotti, G.; Ryckaert, J. *Comput. Phys. Rep.* **1986**, *4*, 345–392.

(21) Williams, D. E. *J. Chem. Phys.* **1967**, *47*, 4680.

(22) Press, W.; Eckert, J. *J. Chem. Phys.* **1976**, *65*, 4362.

(23) Becke, A. D. *J. Chem. Phys.* **1993**, *98*, 5648–5652.

(24) Lee, C.; Yang, W.; Parr, R. G. *Phys. Rev. B: Condens. Matter Mater. Phys.* **1988**, *37*, 785–789.

(25) Hutter, J.; Alavi, A.; Deutch, T.; Bernasconi, M.; Goedecker, S.; Marx, D.; Tuckerman, M.; Parrinello, M. CPMD; MPI für Festkörperforschung and IBM Zurich Research Laboratory: Stuttgart, 1995.

(26) Mugnai, M.; Cardini, G.; Schettino, V. *J. Chem. Phys.* **2004**, *120*, 5327.

(27) Troullier, N.; Martins, J. L. *Phys. Rev. B: Condens. Matter Mater. Phys.* **1991**, *43*, 1993–2006.

(28) Sprik, M.; Hutter, J.; Parrinello, M. *J. Chem. Phys.* **1996**, *105*, 1142.

(29) Nosé, S. *J. Chem. Phys.* **1984**, *81*, 511–519.

(30) Hoover, W. G. *Phys. Rev. A: At., Mol., Opt. Phys.* **1985**, *31*, 1695.

(31) Martyna, G. J.; Klein, M. L.; Tuckerman, M. *J. Chem. Phys.* **1992**, *97*, 2635.

(32) Mazari, N.; Vanderbilt, D. *Phys. Rev. B: Condens. Matter Mater. Phys.* **1997**, *56*, 12848–12865.

(33) Silvestrelli, P.; Mazari, N.; Vanderbilt, D.; Parrinello, M. *Solid State Commun.* **1998**, *107*, 7–11.

(34) Silvestrelli, P. L. *Phys. Rev. B: Condens. Matter Mater. Phys.* **1999**, *59*, 9703–9706.

(35) Berghold, G.; Mundy, C.; Romero, A.; Hutter, J.; Parrinello, M. *Phys. Rev. B: Condens. Matter Mater. Phys.* **2000**, *61*, 10040–10048.

(36) Avrami, M. *J. Chem. Phys.* **1939**, *7*, 1103.

(37) Avrami, M. *J. Chem. Phys.* **1940**, *8*, 212.

CT700275V